Fizika Nizkikh Temperatur, 1997, v. 23, No 7, p. 738–745

Metallic point contacts formed by physical vapor deposition and chemical vapor deposition: microscopy study and point-contact spectroscopy

N. N. Gribov[1,2], J. Caro[1], T. G. M. Oosterlaken[1], and S. Radelaar[1]

[1] *Delft Institute of Microelectronics and Submicron Technology (DIMES), Delft University of Technology, Lorentzweg 1, 2628 CJ Delft, The Netherlands*

[2] *B. I. Verkin Institute of Low Temperature Physics and Engineering, Academy of Sciences of Ukraine, 47 Lenin Ave., Kharkov 310164, Ukraine*
E-mail: gribov@dimes.tudelft.nl

Submitted October 23, 1996

We have made an electron-microscopy study of nanoholes in membranes in successive stages of metal deposition using two different techniques: physical vapor deposition (PVD) and chemical vapor deposition (CVD). One-sided PVD (thermal evaporation) of gold and silver was used, as is relevant for heterocontacts. The key results in this case are: 1) the holes are not filled during deposition and 2) closing of the holes is accomplished by lateral growth of the film on the membrane. In the case of CVD of tungsten we found that nanoholes in membranes are filled at the beginning of the deposition, and that the process is capable of filling holes as small as 10 nm. Fabricated devices (α-tungsten) show good quality point-contact spectra which are characteristic of ballistic transport through the constriction. A very interesting stepwise current increase was observed for one amorphous tungsten point contact.

PACS: 85.30.Hi

1. Introduction

Very stable metallic point contacts (PC) can be made with nanofabrication techniques [1,2]. The contacts are made by metal deposition on both sides of a thin silicon nitride membrane with a hole of diameter in the range 10–30 nm. In this way the nanohole is filled with metal and the electrodes are formed. By using nanofabricated contacts as microscopes of electronic transport, several new, subtle phenomena have been discovered, e.g., two-level resistance fluctuations due to defect motion in the constriction [3,4] and nonuniversal conductance fluctuations involving electron scattering at remote defects [5,6].

Until a few years ago, nanofabricated point contacts were almost exclusively fabricated as homocontacts, i.e., contacts made of the same (very pure) metal. Recently, however, devices of a more complex structure have also been fabricated and studied. Examples are heterocontacts [7,8], contacts including magnetic multilayers [9] and tunnelling contacts [10]. To interpret the electrical transport measurements on these devices and to judge further capabilities of the nanofabrication technique of point contacts, it is crucial to know how the actual contact is formed. About this matter virtually nothing is known, so that one can only guess about the structure and morphology of the constriction region.

In this paper we report an electron-microscopy study of the closing and/or filling of nanoholes in membranes in successive stages of metal deposition and we present the point-contact spectra of the fabricated devices. The deposition techniques used are physical vapor deposition (PVD) and chemical vapor deposition (CVD). Physical vapor deposition, in this case thermal evaporation of Au and Ag from a boat, is the usual technique used to form lithographic point contacts. Chemical vapor deposition is intensively applied in integrated circuit fabrication to deposit semiconductors, insulators, and conductors. Here we use CVD of W, which is well known from the filling of vias (i.e., contact channels to devices or lower-level metallization) in integrated circuits [11], but which so far was not used to produce metallic point contacts. We combine the

results of scanning electron microscopy (SEM) and transmission electron microscopy (TEM) with point-contact spectra of fabricated contacts, thus presenting the complete picture of contact formation and the resulting electrical properties.

2. Electron microscopy study

Microscopy samples were prepared by patterning arrays of holes. Each hole forms from single-pixel exposure with an *e*-beam writer of *e*-beam sensitive resist on a silicon nitride layer. After the resist development holes in resist are transferred to the nitride by etching in an SF_6/He plasma. Etching is stopped when the resist is completely consumed and the nitride thickness is about 25 nm. Depending on whether a sample is prepared for SEM or for TEM, the nitride layer either is initially supported by silicon across the whole area or is a membrane as used for real point contacts [2], respectively. In the case of SEM samples we used arrays of 750×750 holes placed on an 80-nm period square grid. The large extent of this array facilitates breaking of the chip through a «line of holes». The supporting Si is very helpful here, since it is the Si chip that we break along a proper line. In the case of TEM samples we used a 200-nm period array of 7×5 holes in the membrane.

First, with the SEM inspection, we investigated how a hole is filled and/or covered during one-sided PVD of a 200-nm-thick Au or Ag layer, with the substrate oriented perpendicular to the evaporation beam. Before deposition, the substrate is cleaned *in situ* with an O_2 glow discharge. The chamber pressure, substrate temperature, and deposition rate are $5{\cdot}10^{-7}$ Torr, 300 K, and 0.3–0.5 nm/s, respectively. The micrographs in Figs. 1,*a* and 1,*b* show the resulting cross sections. As can be seen, the nitride surrounding a hole is severely underetched. This results from the high isotropic etch rate of Si in the SF_6/He plasma. Effectively, each hole is in a (small) membrane, just like a hole of a real contact. The rounded profile of a hole arises from transferring the resist profile to the nitride and from subsequent overetching. The smallest diameter of a hole is 25 nm. The step coverage of the Ag film is very poor (see Fig. 1,*b*): The film covers the hole, but does not fill it. This finding agrees with the fact that vias of microelectronic devices cannot be filled reliably with metal by PVD [11]. Inspection of the outer Ag surface revealed an array of shallow pits, which result from the missing material that has passed through the holes before closing. In the case of PVD of a 200-nm Au layer we made very similar observations.

Fig. 1. SEM micrographs of the cross sections through a «line of holes», before deposition (*a*) and after deposition of 200-nm Ag (*b*). The voids result from etching in the SF_6/He plasma. At the bottom of the voids in (*b*) some Ag is deposited. Small disturbances of the cross sections may exist as a result of breaking. Dots guide the eye in following interfaces/surfaces.

As a further step we monitored with high-resolution TEM the growth of Au and Ag in successive stages of PVD on membranes with an array of holes of diameter in the range 30–70 nm. Figure 2 shows TEM micrographs in three stages of PVD of Au. From these micrographs and similar ones in other deposition stages we make the following observations.

1. In the initial stage of PVD ($\approx$ 2 nm on thickness monitor, i.e., $1.2{\cdot}10^{16}$ atoms/cm^2; Fig. 2,*a*) grains on the unpatterned membrane parts and on the outer rounded wall of a hole have a certain density. However, a circular region close to the narrowest part of a hole is decorated with a necklace of smaller grains, which have a higher area density.

Fig. 2. TEM micrographs of membranes with holes after deposition of 2, 5, and 20-nm Au (*a*,*b*, and *c*, respectively). A necklace of small grains in the narrow part of the hole is discernible in (*a*) and (*b*). Closing of the hole is accomplished by lateral growth of the film. The bar marker in (*c*) is the same as in (*a*) and (*b*).

2. Grains on the membrane and on the rounded walls coalesce in a way characteristic of an amorphous substrate (≈ 5 nm, i.e., $2.9 \cdot 10^{16}$ atoms/cm^2; Fig. 2,*b*). Since these grains grow faster than the necklace grains, they cannot coalesce with the regular grains in the broader area around a hole.

3. During the stage of formation of a closed polycrystalline film on the membrane (≈ 20 nm, i.e., $11.8 \cdot 10^{16}$ atoms/cm^2; Fig. 2,*c*) closing of a hole occurs by lateral growth of the film. Also for these deposition experiments the observations for Au and Ag were very similar, even though the Ag exposures required to reach the stages of nucleus growth and grain coalescence are approximately twice those of Au.

On TEM micrographs we measured the remaining hole size after deposition of Au layers of different thicknesses. Figure 3 shows the resulting dependences. In the initial stage of deposition the size of the holes decreases very rapidly as a result of formation of the necklace. Further size decrease proceeds slowly. It can be seen that for an initial diameter of 30 nm one should deposit about 70-nm Au to close the hole, i.e., a layer more than twice as thick as the hole diameter.

To investigate the capabilities of CVD to fill holes for point contacts, we also performed TEM analysis of membranes with holes onto which W was deposited by CVD. In particular, we deposited α-W (common bcc W), which we normally apply as interconnect material in microelectronic devices [11]. Depositions of α-W were carried out in a cold-wall, low-pressure CVD reactor by the reduction of WF_6 by H_2 . Films deposited with this process have very good step coverage and a low resistivity. We used a 4″ quartz dummy wafer with slits to accommodate 6×9-mm^2 chips with eight membranes. The slits were machined to leave open a 1-mm gap between the chips and the heater plate of the reactor, to give the reactants free access to the lower face of the membrane. A substrate cleaning step was not included, since we assumed that dry etching in SF_6/He plasma, which is stopped when the resist is consumed and the membranes are thinned to their final thickness, leaves a clean surface. The deposition parameters are T = 500 °C

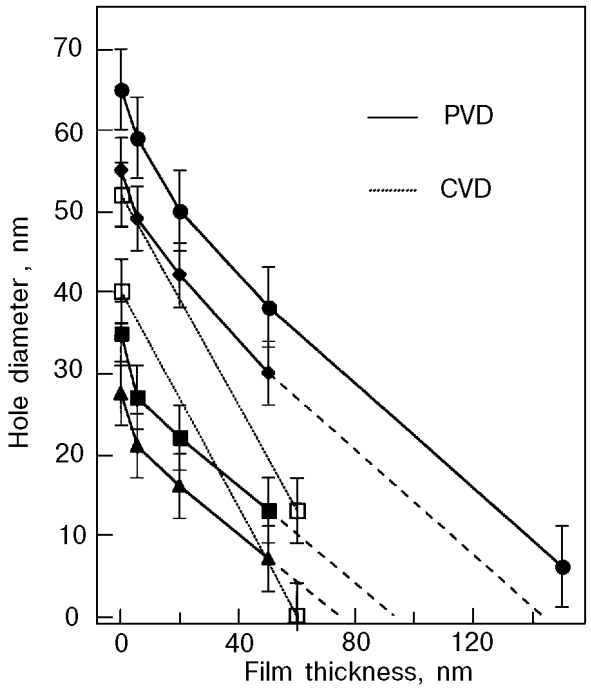

Fig. 3. Remaining hole size (average over membranes and directions) as a function of Au thickness deposited by PVD on one side of a membrane, for four initial hole diameters (filled symbols) and the corresponding depedences for CVD of W, for two initial hole diameters. Error bars result from differences between membranes and measurement directions. Dashed segments are extrapolations.

Fig. 4. TEM micrographs of membranes with holes after CVD of α-W during 30, 40, and 50 s (*a, b*, and *c*, respectively). The bar marker in (*a*) is the same as for (*b*) and (*c*). The arrows in (*c*) indicate the holes which are already closed.

$p = 1$ Torr, 50 sccm WF_6 , and 500 sccm H_2 . The deposition times were 30, 40, 50, and 60 s (20 s appeared to be below the incubation time for nucleation).

In Fig. 4 we show TEM micrographs for deposition times 30, 40, and 50 s. In the initial stage (Fig. 4,*a*) grains occur at the edge of and inside the holes. Holes are filled, therefore, at the outset of the deposition. This is in strong contrast with the above PVD results. Figure 4,*b* shows the next stage, where filling of channels between regions of coalesced grains occurs and where grains and the smallest holes have approximately the same size. A substantial size decrease of some holes occurs already, although the film is not yet continuous. Again, this is in contrast with the results for PVD. The holes used here are much smaller than the structures presently filled with W in microelectronic industry [12]. Nevertheless, Figs. 4,*a* and 4,*b* indicate that very good step coverage develops. For a deposition time of 50 s (Fig. 4,*c*; thickness ~ 60 nm, as measured with a surface profiler) the smallest holes are completely closed and the film seems continuous.

For the W depositions the film thickness was measured for a deposition time of 50 s. Nevertheless, this enables us to plot two more lines in Fig. 3, for two initial hole diameters. The considerably steeper slope of the lines for W beyond the range, where the necklace for PVD is formed, reflects the differences between PVD and CVD in the closing of a hole.

3. Electrical characteristics

Two different types of heterocontacts were made using PVD of Ag and Al as the final steps of our fabrication scheme [2]. Fabricated point contacts were characterized by measuring the point-contact spectrum $d^2V/dI^2\,(V)$ at the liquid-helium temperature. The spectra were nearly antisymmetric with respect to the bias-voltage polarity. It is known that in the case of ballistic electron transport through the contact (the elastic mean free path l_i of electrons is much larger than the contact size) $d^2V/dI^2\,(V)$ reflects the peculiarities of the phonon density of states of the metals that form the contact. Figure 5 shows the PC spectra of PVD fabricated Ag/Al devices. For type-*A* heterocontacts (the cross section of the device is shown schematically in the inset in Fig. 5) after deposition of 200-nm Ag

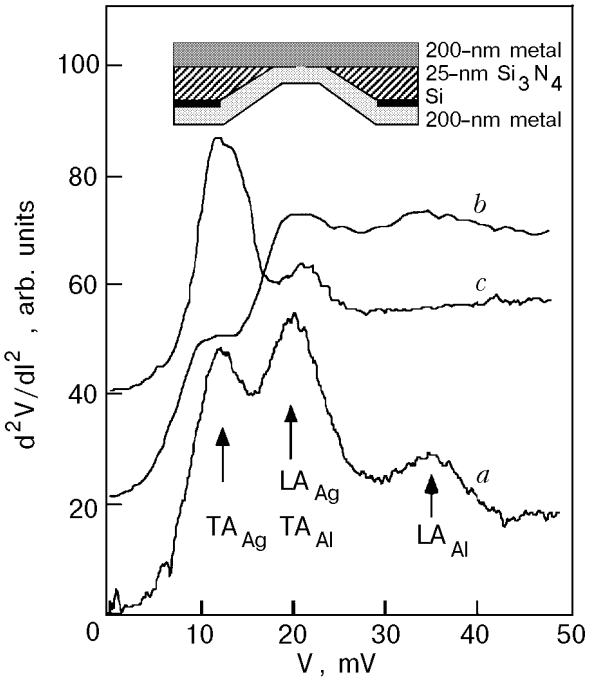

Fig. 5. PC spectra of the Ag/Al heterocontacts described in the text. For a 20-nm-thick Ag layer the phonon peaks from Al are absent. The contact diameters are in the range 10–25 nm. The inset shows a schematic cross section through a point contact.

on side 1 of the membrane with a single nanohole, 200-nm Al was deposited on side 2. One can expect, taking into account the results in Fig. 1, that the Ag/Al interface for this type of heterocontacts is situated close to the center of the constriction, and that the PC spectra should demonstrate the features of both metals. Indeed, as can be seen in Fig. 5,*a*, the point-contact spectrum of a type-*A* device has clear phonon peaks of both Ag and Al. To move the interface Ag/Al away from the constriction, we fabricated type-*B* heterocontacts. For these contacts 200-nm Ag was deposited on side 1 of the membrane and a bilayer of 10-nm Ag/200-nm Al or 20-nm Ag/200-nm Al on side 2. In the case of 10-nm Ag the 35-mV peak of Al is still present in the spectrum (Fig. 5,*b*), but is absent in case of 20-nm Ag. In the latter case the spectrum is that of pure Ag. Similar results were obtained for contacts with 200-nm Al on side 1 and 20-nm Al/200-nm Ag on side 2. For these contacts the spectrum is that of pure Al. A possible explanation for this result is that geometry of our devices is between that of a clean orifice and a short channel. For the last geometry the spectral contribution from the regions outside the channel is reduced compared to that of the clean orifice model, most of the signal coming from the channel region. The results for the heterocontacts with a displaced interface seem to agree with this conclusion. However, the spectral intensities of our homogeneous contacts follow the theoretical relation for the clean orifice model [4], which indicates that the degree of channel character is negligible. Therefore, since the thinner layer of the bilayer is comparable to the probing depth, this result remains unexplained.

From studies of metallization of vias in microelectronic devices it is known that the CVD method is capable of filling holes as small as 70 nm [12]. In order to further investigate the capabilities of W-CVD to fill much smaller holes we have fabricated α-W and amorphous W point contacts with a good yield of devices for electrical measurements. In the case of amorphous W we used the reduction of WF_6 by GeH_4 with the deposition parameters: $T = 300$ °C, $p = 1$ Torr, 50 sccm WF_6, 50 sccm GeH_4, and 500 sccm H_2. In contrast to α-W, the films deposited to by this process have a high resistivity as a result of relatively large concentration of incorporated germanium. The film thickness (per side) was about 350 nm for α-W and 175 nm for amorphous W.

Figure 6 shows a point-contact spectrum of an α-W device of resistance $R = 45.6$ Ω. The contact diameter is $d = 10$ nm (estimated from the Wexler formula), which is much smaller than the size of the

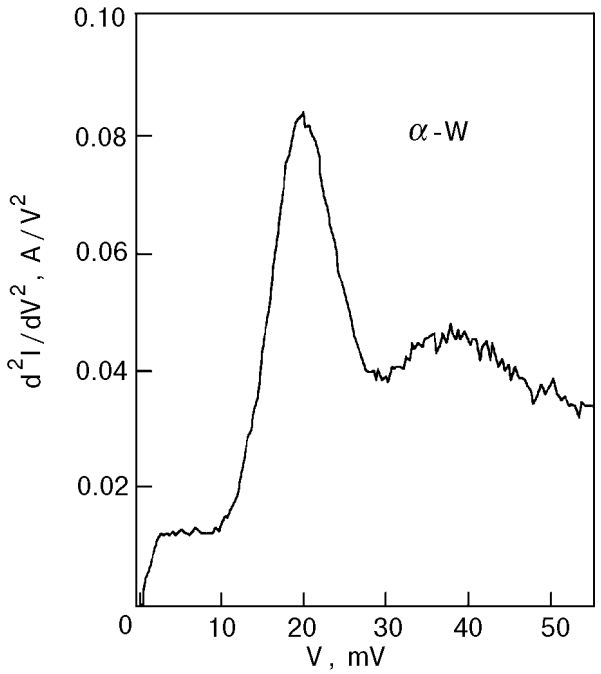

Fig. 6. Point-contact spectrum of an α-W device formed by chemical vapor deposition. $T = 1.5$ K and $R = 45.6$ Ω.

contact plugs used now in microelectronics. The spectrum shows a sharp TA-phonon peak at 20 mV and a weaker and broader feature at 40 mV, which is a double-phonon peak. The background is relatively low and there is a weak zero-bias anomaly. Finally, the LA-phonon peak is not resolved, which is not unusual for α-W contacts [13,14]. The W spectrum in Fig. 6 is comparable to the best spectra of ballistic mechanical point contacts made from a high-purity W base material [13,14]. This indicates that the CVD deposited α-W is of high quality. Indeed, an estimate of the elastic mean free path from the ratio $R_{300K}/R_{4.2K}$ of the film (in the free electron approximation) gives $l_i = 95$ nm, confirming the ballistic transport through the contact.

Bulk layers of amorphous W deposited with CVD are superconducting below 4.3 K, which makes it possible to study the superconducting properties of contacts of this material. To characterize the amorphous W point contacts, we measured the $I-V$ curve and its second derivative d^2V/dI^2 (V) above and below the superconducting transition temperature for several devices. Above T_c the amorphous W contacts appeare to be not very interesting, because the point-contact spectra are virtually structureless. This is a result of the high resistivity of the material (150–200 mΩ·cm at 4.2 K) and the related very short elastic mean free path ($l_i \approx 1$ nm). Below T_c the curves show a rich variety of features which are related to the superconducting state (since they are absent above T_c),

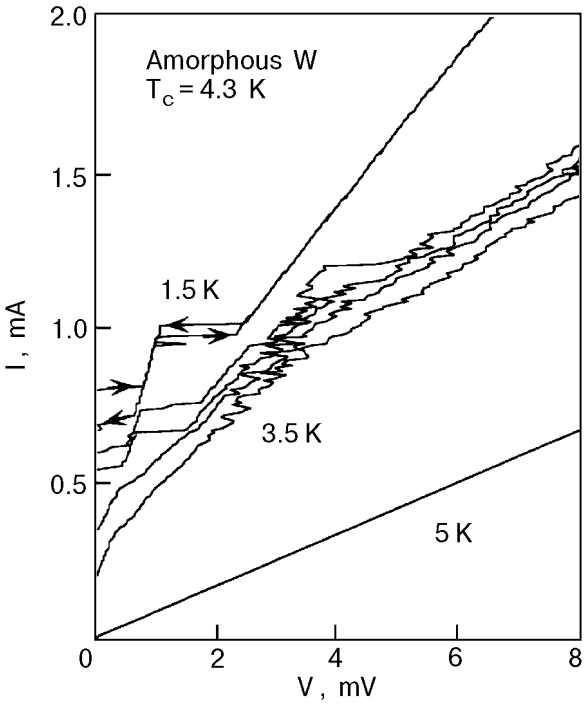

Fig. 7. The $I-V$ characteristics of an amorphous W point contact of $R_N = 12.2\ \Omega$, measured at different temperatures. The estimated contact diameter is 125 nm. Below 4.3 K the curves display a supercurrent.

which could not be classified in a systematic way. We attribute this circumstance to device-dependent compositional inhomogeneities on the scale of the constriction, which arise from the incorporated Ge atoms.

Figure 7 shows examples of $I-V$ curves of an amorphous W point contact with normal state resistance $R_N = 12.2\ \Omega$ and a diameter of 125 nm in the range 1.5–5 K. The contact is characterized by $\xi = 15$ nm and $\lambda \approx 500$ nm. These values were estimated from Gor'kov's relations for dirty superconductors [15] (ξ is the coherence length and λ is the penetration depth). Consequently, the device operates in the dirty transport limit, where $\xi, l_i << d << \lambda$. Below 4.3 K the contact is in the superconducting state and the curves have some structures, in particular, instabilities and a stepwise current increase at low currents. A significant hysteresis was observed when sweeping the current in the opposite direction (see the 1.5-K curve). The sign of the hysteresis was found to be random. From more accurate measurements we found that in the range of a steep current increase the voltage may switch rapidly between two discrete levels, indicative of a transition between two metastable states.

The stepwise behavior is reminiscent of similar behavior in narrow ($\xi, \lambda <<$ width) superconducting channels [16,17]. This behavior was, among other things, explained in terms of phase-slip centers (PSC). Our amorphous W point contacts, however, operate in a different limit than those channels, so that the PSC model does not apply. The origin of the steps in Fig. 7 is probably of mesoscopic nature. To the best of our knowledge, this would be a new aspect of this type of $I-V$ curves, which we will discuss further.

We assume that the stepwise behavior may be related to the motion of vortices created near the entrance of the constriction by the magnetic field generated by the transport current. Although $\lambda >> d$, the formation of such vortices is possible, since $\xi << d$ (ξ is a measure of the vortex core, whose characteristics in this case may be slightly different from those of the Abrikosov vortices). At large enough currents the device resistance would arise from the motion of the vortices. It is known that vortex motion can be blocked by pinning centers, which are expected to be readily available in amorphous CVD-W with built-in germanium. Vortex motion, therefore, is possible only at large enough currents, where the current-induced force overcomes the pinning force. Since the vortex core size (and thus the spatial scale of the pinning relief) is not much smaller than the contact size, one expects a sample-specific percolation-like character of the vortex motion. Increasing the current, therefore, would first lead to the formation of one «path» of vortex motion, which corresponds to a chain of weak enough pinning centers. Then, with an increase of the current, a second percolation path would appear. Accordingly, switching-on of paths would correspond to the steps on the $I-V$ curve, as observed. Of course, this tentative explanation needs further checking.

4. Discussion

The TEM observations for PVD of Au and Ag films on unpatterned parts of the membranes and on the rounded edges of the holes can be explained by applying the growth mechanisms of a metallic film on amorphous substrates [18] and need no further discussion. The main point to be addressed is that, aside from the inner edge region, where the necklace is formed, the holes do not become filled with metal. This can be explained in the following way. The edge of the hole is a part of the substrate with positive curvature (rounded profile; see Fig. 1) and negative curvature (due to the circular shape, as seen in top view). From studies of the metallization of vias in microelectronic integrated circuits it is known [19] that areas of dominating negative curvature are preferential sites for nucleation and

growth. In our case this leads to nuclei close to the narrowest part of the hole and subsequently to the necklace of small grains. Since, the hole is a missing area, the atoms emitted from the melt are lost. This reduces the number of adatoms collected by nuclei near the hole, so that these nuclei grow slower than other nuclei. This effect is even enhanced because of the inclination of the wall of the hole with respect to the incoming atomic beam (increase of area). We believe that the absence of coalesced grains at the inner edge of the hole (see Fig. 2,*b*) and the slower growth of necklace grains are attributable to this mechanism.

After deposition on one side, the metal that covers the hole acts as a microsubstrate during deposition on the other side. TEM inspection after deposition of 20-nm Ag on side 2 (200-nm Ag was deposited on side 1) showed a dark region inside the hole, surrounded by a light halo, while it was not clear that growth had started on the side wall. This suggests preferential growth on the metal inside the contact hole, which after prolonged deposition on side 2 might lead to a (poly) crystal that bulges out of the hole. A 200-nm Al is deposited on the surface of this bulging crystal. This means that the distance of the Ag/Al interface on side 2 to the constriction is equal to the height of the crystal, which can be larger than 20 nm and larger than the expected depth to which the electron-phonon interaction can be probed. If this is true, it may explain the absence of the LA peak in Fig. 5,*c* for the Ag/Al heterocontact with the 20-nm Ag interlayer.

The results for one-sided PVD tempt us to speculate about the fabrication of homocontacts, which are usually formed while rotating the substrate in the beam emerging from the melt. We expect that such a two-sided deposition will not noticeably suppress the tendency of the hole's wall to remain uncovered. However, when a hole starts to close from two sides, edges may continue to grow (as seen from the inside), so that filling starts. Simultaneously, the interior of the hole becomes less accessible, so that filling becomes harder and may not be completed in some cases (void formation). Clearly, this would limit the yield of the fabrication process.

Our electrical measurements on heterocontacts indicate that, in principle, very good devices of this type can be fabricated with PVD. It turns out, however, that deposition of a bilayer on one side of the membrane does not give enough control over the position of the heterointerface. In additions, control over the degree of flatness of the interface, a requirement for detailed studies of interface scattering, is not guaranteed. These findings suggest modifications of the fabrication process. For example, we are considering to form point contacts by first depositing metal 1 (or a bilayer or multilayer of metals) on side 1 of the membrane, followed by a highly selective etch of type hole and finally by depositing metal 2 in the hole and on the reverse side of the membrane.

In the case of CVD the TEM observations can be understood from the properties of this process. First, because the reactive sticking coefficient is small, most of the impinging molecules are reemitted. This circumstance and also the random velocity distribution of the reactants provide a supply of the material to all surface areas, irrespective of the local surface orientation. Thus, the walls of the hole are covered from the beginning of deposition. In turn, for the PVD process the sticking probability is close to unity (no reemission) and, by geometry, the velocity of impinging atoms is mainly directed along the axis of the hole, promoting preferential growth at its entrance.

The electrical data for W contacts indicate that CVD, by nature, is very suitable to fabricate metallic point contacts. A limitation is that CVD processes are available for a limited number of metals. Stimulated by the results on the W contacts, we have recently started the fabrication with CVD of Si point contacts. In this case CVD makes it possible to fabricate completely single-crystalline devices [20].

5. Conclusions

We have made an electron-microscopy study of the closing of nanoholes in membranes at the successive stages of one-sided physical vapor deposition of Au and Ag, as it occurs in heterocontact formation. We is found that the holes do not become filled with metal in a one-sided deposition. The holes are closed by lateral growth of the film on the membrane when its thickness is more than twice the hole diameter. Metal closing of one side of a hole serves as a microsubstrate for growth of metal deposited from the other side. Growth from the other side seems to occur preferentially on the metal and not on the side walls.

We have also applied chemical vapor deposition of α-W and amorphous W to the formation of point contacts. From TEM inspections we find that the W-CVD process is capable of filling holes as small as 10 nm from the beginning of the deposition, in contrast to physical vapor deposition. Fabricated devices show good quality point-contact spectra of electron-phonon interaction, conforming that PVD and CVD processes yield ballistic point contacts.

For one amorphous W device we have observed a very interesting stepwise current increase which may arise from switching-on of percolation paths for vortex motion.

This work is a part of the research program of the Stichting voor Fundameteel Onderzoek der Materie (FOM), which is financially supported by the Nederlandse Organisatie voor Wetenschappelijk Onderzoek (NWO). N. N. Gribov acknowledges the NWO for a grant received in a program for scientists of the former Soviet Union (ref. no. 714-033). We appreciate valuable comments of Oleg Shklyarevskii. We thank C. D. de Haan of the National Centre of High Resolution Electron Microscopy of Technical University of Delft for TEM analyses.

1. K. S. Ralls, R. A. Buhrman, and R. C. Tiberio, *Appl. Phys. Lett.* **55**, 2459 (1989).
2. P. A. M. Holweg, J. Caro, A. H. Verbruggen, and S. Radelaar, *Microelectronic Engineering* **11**, 27 (1990).
3. K. S. Ralls and R. A. Buhrman, *Phys. Rev. Lett.* **60**, 2443 (1988).
4. P. A. M. Holweg, J. Caro, A. H. Verbruggen, and S. Radelaar, *Phys. Rev.* **B45**, 9311 (1992).
5. P. A. M. Holweg, J. A. Kokkedee, J. Caro, A. H. Verbruggen, S. Radelaar, A. G. M. Jansen, and P. Wyder, *Phys. Rev. Lett.* **67**, 2549 (1991).
6. P. A. M. Holweg, J. Caro, A. H. Verbruggen, and S. Radelaar, *Phys. Rev.* **B48**, 2479 (1993).
7. N. N. Gribov, J. Caro, and S. Radelaar, *Physica* **B218**, 97 (1996).
8. D. C. Ralph, *Ph. D. Thesis*, Cornell University (1994).
9. R. Louie, S. Upadhyay, and R. A. Buhrman, *Bull. Am. Phys. Soc.* **41**, 304 (1996).
10. D. C. Ralph, C. T. Black, and M. Tinkham, *Phys. Rev. Lett.* **74**, 3241 (1995).
11. E. H. A. Granneman, *Thin Solid Films* **228**, 1 (1993).
12. T. Ohba, *MRS Bull.* **XX**, 46 (1995).
13. J. Caro, R. Goehoorn, and D. G. de Groot, *Solid State Commun.* **39**, 267 (1981).
14. L. F. Rybal'chenko, I. K. Yanson, N. L. Bobrov and V. V. Fisun, *Sov. J. Low Temp. Phys.* **7**, 82 (1981).
15. L. P. Gor'kov, *Sov. Phys. JETP* **9**, 1364 (1959).
16. A. Barone and G. Paterno, *Physics and Applications of the Josephson effect*, Willey, New York (1982).
17. T. M. Klapwijk, M. Sepers, and J. E. Mooij, *J. Low Temp. Phys.* **27**, 801 (1977).
18. D. W Pashley, M. J Stowell, M. H. Jacobs, and T. J. Law, *Philos. Mag.* **10**, 127 (1964).
19. T. Smy, S. K. Dew, and M. J. Brett, *presented at a course in conjunction with the Advanced Metalization Conference in Texas* (1994).
20. J. W. H. Maes, J. Caro, C. C. G. Visser, T. Zijlstra, E. W. J. M. van der Drift, S. Radelaar, F. D. Tichelaar, and E. J. M. Fakkeldij, *Appl. Phys. Lett.* **70**, 973 (1997).